Letter

Magnetic signature of thermoelectric cardiac dynamics

Anna Crispino,[1,*] Martina Nicoletti,[1,2,*] Alessandro Loppini,[3,†] Alessio Gizzi,[2] Letizia Chiodo,[1,4] Christian Cherubini,[5] and Simonetta Filippi[1,4]

[1]*Department of Engineering, Università Campus Bio-Medico di Roma, I-00128 Rome, Italy*
[2]*Center for Life Nano and Neuro Science (CLN2S@Sapienza), Italian Institute of Technology, I-00161 Rome, Italy*
[3]*Department of Medicine and Surgery, Università Campus Bio-Medico di Roma, I-00128 Rome, Italy*
[4]*Istituto Nazionale di Ottica del Consiglio Nazionale delle Ricerche (CNR-INO), I-50125 Florence, Italy*
[5]*Department of Science and Technology for Sustainable Development and One Health, Università Campus Bio-Medico di Roma, I-00128 Rome, Italy*

(Received 5 July 2024; revised 31 October 2024; accepted 26 November 2024; published 16 January 2025)

Developing methods to predict electromagnetic instabilities in cardiac dynamics is crucial. However, a comprehensive view of the heart's magnetic activity at a tissue scale is still needed. To address such a challenging problem, we present a theoretical framework to investigate thermoelectric cardiac dynamics from the magnetic field perspective. Our framework demonstrates that periodic stimulations of cardiac cell strands create an external magnetic field, revealing predictable features of nonlinear spatiotemporal cardiac dynamics. Magnetic restitution curves better discriminate instabilities and bifurcations through a thermo-electro-magnetic map analysis. This new approach lays the foundation for innovative, noninvasive diagnostic tools for cardiac arrhythmias.

DOI: 10.1103/PhysRevE.111.L012401

Introduction. Over the past 50 years, the adoption of preventive strategies targeting cardiac risk reduction has significantly decreased mortality from cardiovascular causes [1,2]. Despite this considerable progress, cardiovascular diseases remain the leading cause of death in developed countries, with sudden cardiac death (SCD) constituting approximately half of all cardiac-related fatalities [3,4]. In this scenario, understanding the basic mechanisms for identifying risk factors and therapeutic approaches is critical to diagnosing, preventing, and managing cardiac arrhythmias. Electric instabilities in cardiac dynamics, arising in the form of action potential alternans in time and space [5–10], are well-established precursors of arrhythmias related to SCD [11–13]. Spatiotemporal oscillations are attributed to multiscale and multiphysics factors, starting from cellular-level ion dynamics, comprising inherent tissue heterogeneity and anisotropy, and entailing external factors like thermomechanical variation [14–20]. Increased body temperature occurs in the case of fever, sports fatigue, heat strokes, and in medical practice, in the case of whole-body hyperthermia induced to improve the chemotherapy success rate. Low body temperatures are used in medical practice to minimize cellular damage. Specifically, thermal monitoring is widely used as a therapeutic intervention to prevent injuries associated with cardiac arrest [21]. Body temperature can also decrease dramatically during accidents such as avalanches and ship sinkings, for instance. From a cellular point of view, changes in body temperature result in oscillation in action potential duration (APD), which is considerably increased at low temperatures [Fig. 1(b)]. In cardiac electrophysiology, a one-dimensional map, known as the restitution curve, can be defined [Fig. 1(a)] [22,23] to describe how the APD depends on the recovery phase between each cardiac cycle, thatis, the diastolic interval (DI), or, alternatively, on the stimulation period, that is, the pacing cycle length (PCL) (Fig. S1 in Supplemental Material [24]). The analysis of restitution curves provides valuable insights into the dynamical behavior of cardiac electrical activity, describing the transition between normal and arrhythmogenic regimes. These regimes are distinguished in the restitution curves by changes in the slope s. Steep regions, with $|s| > 1$, are, indeed, associated with beat-to-beat oscillation, that is, alternans, leading to conduction block or spiral wave breakup [25,26]. On the other hand, in smooth regions ($|s| < 1$), the beat rhythm is physiological.

The coordinated electrical activity resulting from the AP propagation gives rise to a magnetic field [Fig. 1(c)]. This field arises from the diffusive currents that accompany AP propagation, and its characteristics are intrinsically connected to the shape and temporal evolution of the AP signal itself. A fundamental question in the study of cardiac magnetic fields is whether they convey more physical information than the respective electric field, which is investigated with standard and well-established techniques [27]. In the past 60 years, both experimental and theoretical works demonstrated the capability of the magnetic field to reveal information not

*These authors contributed equally to this work.
†Contact author: a.loppini@unicampus.it

Published by the American Physical Society under the terms of the Creative Commons Attribution 4.0 International license. Further distribution of this work must maintain attribution to the author(s) and the published article's title, journal citation, and DOI.

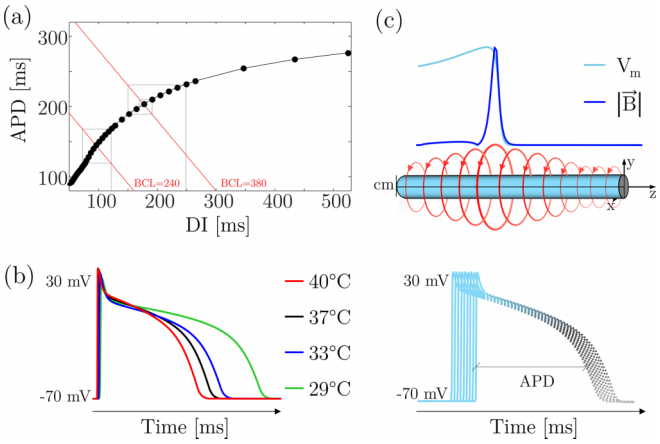


FIG. 1. Schematic representation of (a) Action potential duration-diastolic interval iterated restitution map (black dotted line) with cobweb (grey lines) associated to selected basic cycle lengths (BCL = APD + DI, red lines), (b) thermoelectric morphology of action potential over time at different temperatures, and (c) one-dimensional cylindrical geometry model supporting cardiac action potential spatiotemporal propagation and magnetic field representation. All values of the norm of the magnetic field $|\vec{B}|$ and V_m along the wire are shown at a fixed time step.

found in the electric signature of cardiac excitation [28–31], paving the way for the establishment of magnetocardiography as an advanced technique for the diagnosis of cardiac pathologies [32,33]. An open challenge in the study of cardiac magnetic field is the investigation of magnetic signals at the cellular scale because of their very low intensity (in the pT ÷ nT range) [34–38], posing several experimental challenges. Emerging technologies, such as biocompatible quantum sensing [34,35,38,39], hold promise in shedding light on the molecular origin of biological magnetic fields and, at the same time, to further enhance diagnostic accuracy, potentially transforming the landscape of arrhythmia management in the near future. In this intriguing scenario, mathematical models could significantly contribute to expanding our comprehension of the cardiac function by offering an organic description of the complex interplay of electric and magnetic field dynamics.

In this Letter, we unveil the magnetic features of an excitable biological system by considering a spatiotemporal temperature-dependent cardiac scenario. To introduce such a perspective, we deploy innovative magnetic field–based indicators by selecting a minimal case study represented by a one-dimensional geometry. In this simplified yet representative scenario, our aim is to provide an initial approach to investigating the magnetic effects of temperature on cardiac dynamics. An extended validation of predictability is obtained by comparing and contrasting with standard AP-based indicators (also comprising conduction velocity [CV]), considering a wide range of temperatures, thus contributing to the definition of a novel thermo-electro-magnetic multiphysics theoretical framework.

Methods. Cardiac AP excitation and propagation were obtained using a four-variable phenomenological model, fine-tuned on optical mapping experimental recordings [5], including temperature-related effects [40], and amenable for full pacing-down restitution protocol (see Fig. 1):

$$\begin{aligned}
\partial_t u &= D\nabla^2 u - (J_{fi} + J_{si} + J_{so}) \\
\partial_t v &= \Phi_v(T)\left[(1 - H(u-\theta_v))\frac{v_\infty - v}{\tau_v^-} - \frac{H(u-\theta_v)}{\tau_v^+}\right] \\
\partial_t w &= \Phi_w(T)\left[(1 - H(u-\theta_w))\frac{w_\infty - w}{\tau_w^-} - \frac{H(u-\theta_w)}{\tau_w^+}\right] \\
\partial_t s &= \Phi_s(T)\left[\frac{(1+\tanh(k_s(u-u_s)))/2 - s}{\tau_s}\right].
\end{aligned} \tag{1}$$

Here, the variable u represents the nondimensional membrane potential, while v, w, and s regulate temperature-dependent fast-inward (J_{fi}), slow-inward (J_{si}), and slow-outward (J_{so}) currents (see Supplemental Material [24] for details). The electrical activity is simulated in a one-dimensional geometry, consisting in a 3-cm-long cable containing 300 cells. Current density $\vec{J}$ resulting from AP propagation was estimated using Ohm's law, considering for the sake of simplicity homogeneous and isotropic tissue conductivity σ and a dimensional membrane potential varying in the z coordinate only $V_m(t,z)$ (with current density flowing on the z direction only then—see Supplemental Material [24] for details) [34,41,42]:

$$\vec{J} = -\sigma\nabla V_m \;\longrightarrow\; J_z(t,z') = -\sigma\frac{\partial V_m}{\partial z}. \tag{2}$$

The electrical signals propagating in the system have extremely slow variations compared with signals moving at the speed of light, allowing us to neglect any electromagnetic wave phenomena and safely use magnetostatic formulas of classical electromagnetism adapted to the present framework. Having in mind a straight cylinder in the z-direction with $z' \in [z_{\min}, z_{\max}]$ (Fig. 1), with an orthogonal circular section of radius R' in the $x'y'$ plane, denoted by $S' = \pi R'^2$ and $\vec{J} \equiv (0,0,J_z)$, we can adopt standard Biot-Savart's law to obtain the magnetic field $\vec{B}_0$ originated by the diffusive currents in the z direction. We evaluated the magnetic field at a distance of 50 μm from the source, which is consistent with experimental setups using nitrogen-vacancy-center-based magnetometers capable of detecting weak magnetic fields in biological samples [34,35]. This choice, in addition to the quasistatic approximation, allows us to neglect the effect on the magnetic field of induced currents in the surrounding medium, which, in principle, is conductive. In this way, we could significantly reduce the complexity of the magnetic field calculations by assuming the surrounding medium as nonconductive vacuum to a good approximation [34,41].

As usual in the literature, primed quantities refer to the specific source portion location and not primed ones to the position in which the magnetic field is computed, while the corresponding primed and nonprimed Cartesian coordinate systems can be exactly superimposed.

For the sake of simplicity, the section is considered infinitesimal such that a one-dimensional current source approximation along the z-axis can be made. Accordingly, J_z is constant along the z-orthogonal section, and $I(t,z') = \int_{S'} \vec{J}(t,\vec{r}\,') \cdot d\vec{S}' = J_z(t,z')\pi R'^2$. Using Biot-Savart's law for a

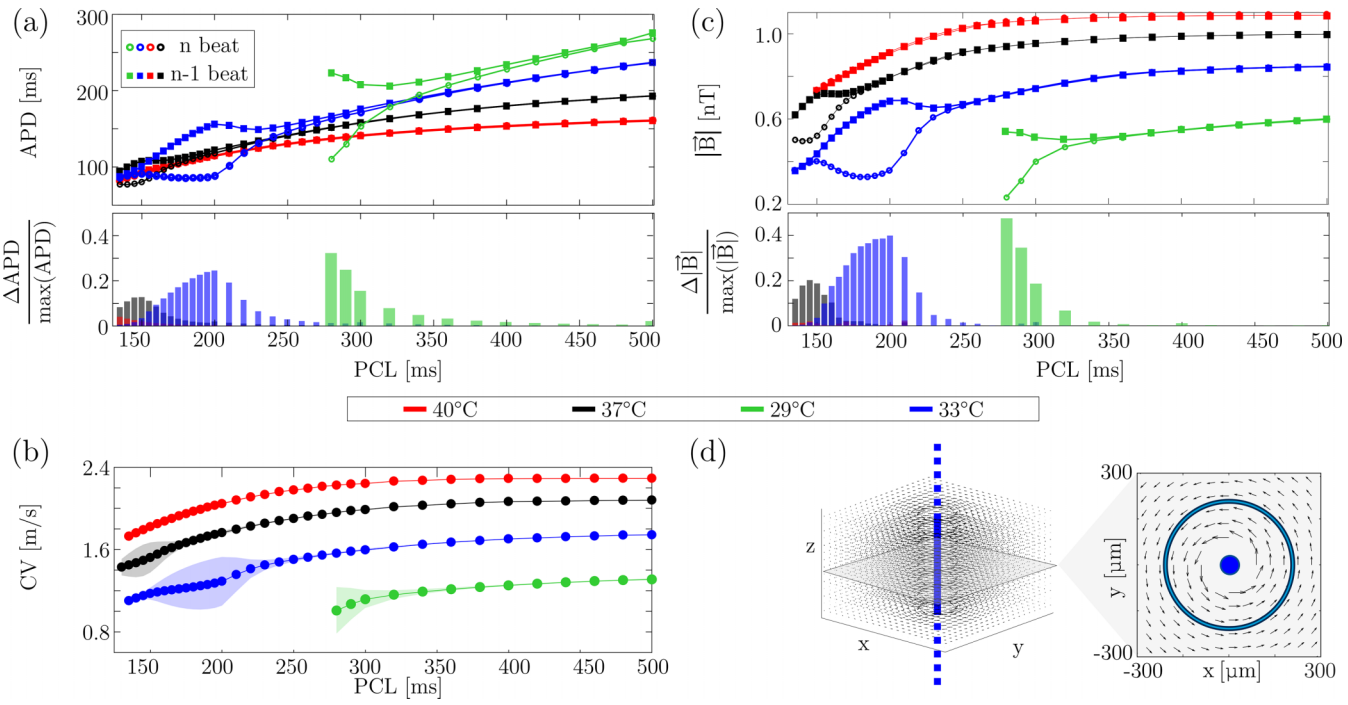


FIG. 2. Restitution curves of (a), (top) action potential duration, (b) conduction velocity (mean ± standard deviation, represented as shaded area), and (c), (top) magnetic field norm at four different temperatures (40°C to 29°C). Bar plot representing normalized differences between action potential duration (a), (bottom) and $|\vec{B}|$ (c), (bottom) are shown. Panel (d) shows the superimposition at different time frames of the three-dimensional magnetic field configuration at 37°C, including the two-dimensional representation in the *xy* plane for a selected *z* coordinate. The blue annular ring represents a typical spatial grid for computing the magnetic field norm.

zero-thickness wire:

$$\vec{B}_0 = \frac{\mu_0}{4\pi}\int_{z_{\min}}^{z_{\max}} \frac{I(t,z')d\vec{l}' \wedge \Delta\vec{r}}{|\Delta\vec{r}|^3}, \tag{3}$$

with $\Delta\vec{r} = \vec{r} - \vec{r}\,'$, $\vec{r} = (x,y,z)$, $\vec{r}\,' = (0,0,z')$, and $\vec{dl}' = (0,0,dz')$, simple vector analysis ($\hat{i}$ is the x-versor, $\hat{j}$ the y-one) leads to:

$$\vec{B}_0 = -\frac{\mu_0}{4\pi}\int_{z_{\min}}^{z_{\max}} \frac{I(t,z')y\,dz'}{[x^2+y^2+(z-z')^2]^{\frac{3}{2}}}\hat{i} + \frac{\mu_0}{4\pi}\int_{z_{\min}}^{z_{\max}} \frac{I(t,z')x\,dz'}{[x^2+y^2+(z-z')^2]^{\frac{3}{2}}}\hat{j}. \tag{4}$$

If $z_{\min} \to -\infty$, $z_{\max} \to +\infty$ and $I(t,z') = I_0 = \text{const}$, the previous formula leads to

$$\vec{B}_0 = -\frac{\mu_0 I_0 y}{2\pi(x^2+y^2)}\hat{i} + \frac{\mu_0 I_0 x}{2\pi(x^2+y^2)}\hat{j}, \tag{5}$$

which is the Cartesian coordinate version of the field generated by a thin, indefinite straight wire carrying a constant electrical current (in cylindrical coordinates this is well-known to be $\vec{B}_0 = \mu_0 I/2\pi r\,\hat{\phi}$). If instead, we had worked in a situation in which the section of the wire would have not been negligible, we should have adopted the well-known electromagnetism formula:

$$\vec{B}_0 = \frac{\mu_0}{4\pi}\int_{\tau'} \frac{\vec{J}(t,\vec{r}\,') \wedge \Delta\vec{r}}{|\Delta\vec{r}|^3}\,d^3x', \tag{6}$$

requiring more involved multidimensional integrals on the volume τ' of the wire. Incidentally, expanding in Taylor series the previous formula on the point $\vec{r}\,' = (0,0,z')$, keeping the zero-order term, and integrating $dx'dy'$ on the orthogonal sections S', one easily recovers Eq. (4).

Magnetic restitution values were extrapolated for each PCL by determining the peak value across the complete temporal span of each beat ($n-1$ and n beats) and the entire length of the wire, within a 50 μm radius from the wire's center [Fig. 2(d)]. APD_{80} restitution curves were considered by thresholding simulated signals at 80% of repolarization and averaging over the entire wire length for each PCL.

Results. Traditional indicators based on AP features, specifically APD and CV, are here evaluated and compared with novel indicators derived from the magnetic field signal (Fig. 2). As an alternative to the classical APD restitution curves, we propose a new approach based on the magnetic field norm, aiming to provide a distinct and energetic perspective on dynamic instabilities in the heart.

The APD restitution curves [Fig. 2(a)] display the expected behavior [18,20,40] with increasing APD, decreasing CV, and early alternans onset at low temperatures. Interestingly, the magnetic restitution curves [Fig. 2(c)] appear to be reliable and effective tools for detecting beat-to-beat changes in the AP during alternans. Magnetic field restitution curves [Fig. 2(c)] confirm a peak value between $0.1 \div 1$ nT, in line with the literature [34,36–38], with the amplitude decreasing as the temperature and PCL lower [Fig. 2(c)]. Such an effect is due to the slowing of AP propagation and the smoothing of the AP depolarization and repolarization wavefronts, reducing

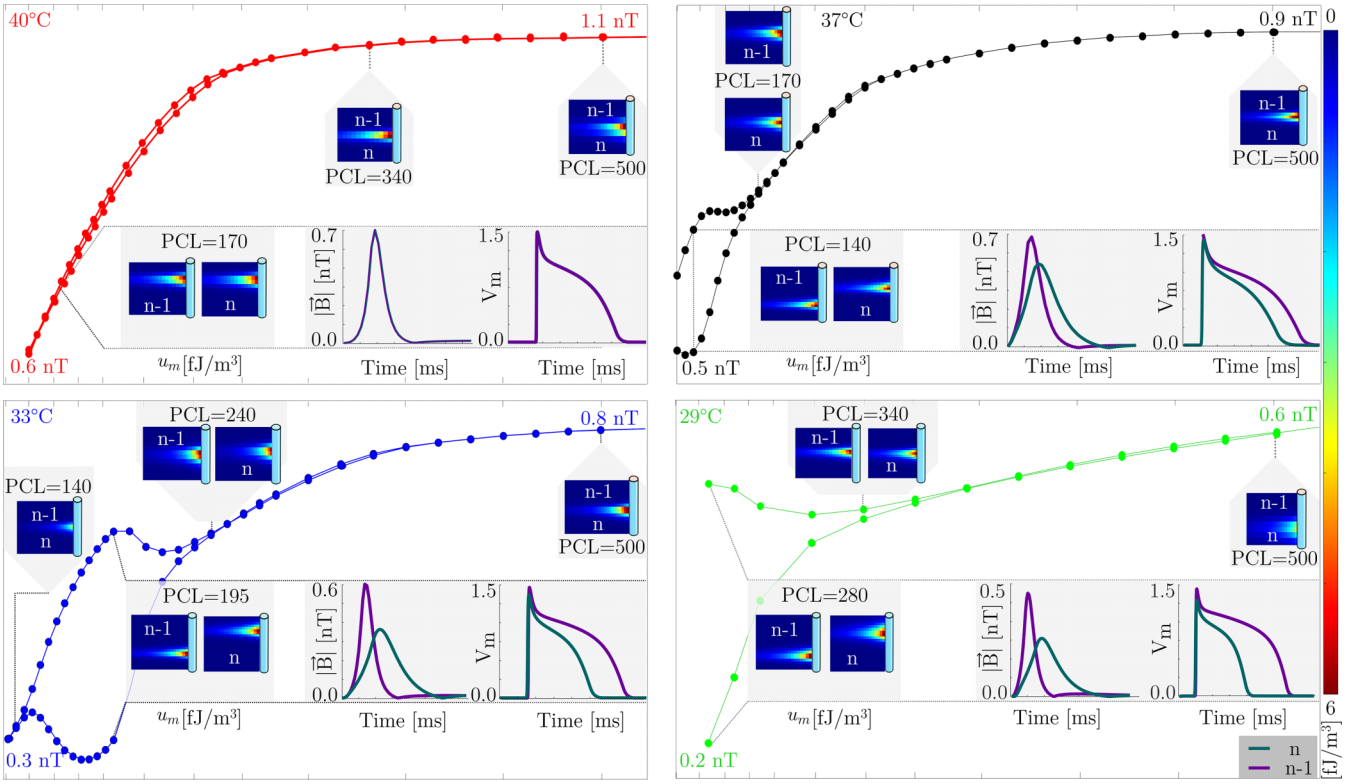


FIG. 3. Representation of the magnetic energy distribution along the magnetic restitution curves at four temperatures (40°, 37°, 33°, 29°). In each panel, the restitution curve is plotted together with the color plot of the distribution of the magnetic energy density (u_m [fJ/m^3]) along the wire for three selected pacing cycle lengths representative of steady-state, alternans onset, and maximum alternans amplitude, respectively. Also, in the inset of each panel, for the maximal alternans amplitude, we show the action potentials and magnetic field norm for the n (in green) and $n-1$ (in purple) beat.

the intensity of magnetic field sources at the cellular level, that is, diffusive currents (Supplemental Material Fig. S2). Indeed, the upstroke velocity [represented by $(\partial V_m/\partial t)_{\max}$, Supplemental Material Fig. S2] strongly affects the spatial and temporal gradients of membrane voltage, and thus the current density generating the magnetic field. For further details on the relation between the maximal value of $|\vec{B}_0|$ and the AP waveform, we refer the reader to the Supplemental Material [24].

Beat-to-beat variations in cardiac activation maps appear both for the electrical-based indicators and the magnetic field capturing alternans regimes, whose onset is quantified by bifurcation points on restitution curves. In this regard, we compared the propensity of the indicators in highlighting alternans by computing the difference in their normalized value between consecutive beats at different temperatures (Figs. 2(a) and 2(c), lower panels). It is well-established that hypothermic conditions promote alternans onset, as indicated by the earlier bifurcation at lower temperatures. This effect is even more pronounced in the magnetic field maps, where the maximum normalized beat-to-beat difference is ∼50%, compared with ∼30% for the APD. Such a result suggests that magnetic field–based indicators are more sensitive in detecting deviations within spatiotemporal dynamics.

To comprehensively understand alternans' dynamics through a magnetic field perspective, we further characterized the spatial distribution by conducting a cross-temperature analysis of the magnetic energy density $u_m = |\vec{B}_0|^2/(2\mu_0)$. We selected three PCLs representative of nonalternating, bifurcation onset, and maximum alternans amplitude regime, respectively (Fig. 3), thus computing u_m in the surrounding of the wire. In the case of maximum alternans amplitude, we also compared the electrophysiological and magnetic field temporal responses between two consecutive beats. Notably, the magnetic energy distribution mirrored the spatial distribution of the magnetic field at each PCL, showing an increased density in the proximity of the active region where the AP wavefront is localized [Figs. 1(c) and 3]. It is worth noting that the magnetic energy distribution is strongly related to the AP features (Fig. 3). Specifically, short APs (*n-1* beat) produce a broader temporal and spatial distribution of the magnetic field compared with long APs (n beat). In addition, for short APs, we observed a notable decrease in magnetic field intensity and the corresponding spatial energy density. An extended temporal and spatial magnetic activity associated with short APs might be related to a slow depolarization phase, which is, in turn, temperature-dependent (Fig. S2, Supplemental Material [24]) [28]. This relationship is further supported by the similar behaviors observed in the respective restitution curves, reinforcing the hypothesis that the magnetic field intensity serves as a sensitive indicator, effectively capturing and amplifying the underlying electrical dynamics.

Moreover, our findings indicate that, as the temperature decreases, the magnetic energy density appears more distributed along the propagation direction and surrounding regions (Fig. 3). Therefore, a broader spatial distribution of

magnetic activity under hypothermic conditions may further affect the dynamics of cardiac excitation and conduction.

Conclusions. Gaining a deeper comprehension of the origin and progression of cardiac arrhythmias is critical for developing novel diagnostic and therapeutic strategies. In this context, the study of the cardiac magnetic field could offer an exciting perspective that has already revealed its potential at the diagnostic level [43]. However, a magnetic description of cardiac alternans at the cellular level still needs to be included, particularly as far as temperature-related effects are concerned. In this Letter, we aim to bridge the gap between traditional electrophysiological indicators and novel magnetic field measurements from a cellular scale point of view. Considering a minimal system supporting cardiac alternans, novel restitution maps based on the magnetic field were created using fine-tuned experimental-based mathematical modeling. In agreement with state-of-the-art studies highlighting an augmented risk of cardiac alternans at low temperatures [14–20], the magnetic field analysis highlights the onset of alternans and an enhanced beat-to-beat variability (Fig. 2). Our results indicate that magnetic field–based indicators could substitute and even outperform traditional electrical indicators in detecting cardiac alternans, especially at low temperatures. However, it is important to remark that the measurement of the maximal value of $|\vec{B}_0|$ is not the direct equivalent of the APD; rather it is an experimentally accessible measure of the AP upstroke characteristics. Indeed, it is striking that even a simple magnetic field indicator can capture such electrical instability dynamics, which are more challenging to calculate. A strong relation between the magnetic field and cellular electrical activity offers interesting possibilities for noninvasive investigation of cardiac electrophysiology in both healthy and diseased cases. In particular, this study opens interesting possibilities for the study not only of temperature-related disturbances of the heart rhythm but also for the investigation of cardiac dynamics in the ischemic or infarcted regions. Moreover, magnetic field–based investigation of cardiac electrophysiology paves the way for the study of biological samples in physiological conditions, even without direct access to the cells. The analysis of spatial and temporal distribution both of the magnetic field intensity $|\vec{B}|$ and of magnetic energy density u_m in a simple geometry, as the straight wire considered here, could be critical for understanding and optimizing the performance of ultrasensitive devices such as those based on nitrogen-vacancy centers, a particular class of magnetometers well-known for their biocompatibility and ability to operate at room temperature, and relying on the Zeeman effect [44–46]. Consequently, the higher the intensity of $\vec{B}$, the more intense the coupling between the magnetic field and spin of the quantum sensor and, therefore, the observed splitting in the electron spin resonant spectra. In conclusion, despite the strong simplification of the case study, that is, wirelike geometry, this Letter constitutes a step toward novel perspectives in the study of cardiac dynamics in health and disease.

Acknowledgments. This research was funded by the European Commission-EU under the HORIZON Research and Innovation Action MUQUABIS GA No. 101070546, and by the European Union - NextGeneration EU, within PRIN 2022, PNRR M4C2, Project QUASAR 20225HYM8N [CUP C53D2300140 0008]. The authors wish to acknowledge the Italian National Group for Mathematical Physics, GNFM-INdAM. C.C. and S.F. wish to acknowledge ICRA and ICRANet.

[1] J. Stewart, K. Addy, S. Campbell, and P. Wilkinson, Primary prevention of cardiovascular disease: Updated review of contemporary guidance and literature, JRSM Cardiovasc. Dis. **9**, 2048004020949326 (2020).

[2] J. Rippe, Lifestyle strategies for risk factor reduction, prevention, and treatment of cardiovascular disease, Am. J. Lifestyle Med. **13**, 204 (2019).

[3] Z. J. Zheng, J. B. Croft, W. H. Giles, and G. A. Mensah, Sudden cardiac death in the United States, 1989 to 1998, Circulation **104**, 2158 (2001).

[4] M. Di Cesare, P. Perel, S. Taylor, C. Kabudula, H. Bixby, T. Gaziano, D. McGhie, J. Mwangi, B. Pervan, J. Narula, D. Pineiro, and F. Pinto, The heart of the world, Glob. Heart **19**, 11 (2024).

[5] A. Gizzi, E. Cherry, R. Gilmour, S. Luther, S. Filippi, and F. H. Fenton, Effects of pacing site and stimulation history on alternans dynamics and the development of complex spatiotemporal patterns in cardiac tissue, Front. Physiol. **4**, 71 (2013).

[6] H. Ito and L. Glass, Spiral breakup in a new model of discrete excitable media, Phys. Rev. Lett. **66**, 671 (1991).

[7] M. Courtemanche, L. Glass, and J. P. Keener, Instabilities of a propagating pulse in a ring of excitable media, Phys. Rev. Lett. **70**, 2182 (1993).

[8] H. M. Hastings, F. H. Fenton, S. J. Evans, O. Hotomaroglu, J. Geetha, K. Gittelson, J. Nilson, and A. Garfinkel, Alternans and the onset of ventricular fibrillation, Phys. Rev. E **62**, 4043 (2000).

[9] K. Hall, D. J. Christini, M. Tremblay, J. J. Collins, L. Glass, and J. Billette, Dynamic control of cardiac alternans, Phys. Rev. Lett. **78**, 4518 (1997).

[10] G. Bub, A. Shrier, and L. Glass, Global organization of dynamics in oscillatory heterogeneous excitable media, Phys. Rev. Lett. **94**, 028105 (2005).

[11] Z. Qu, G. Hu, A. Garfinkel, and J. N. Weiss, Nonlinear and stochastic dynamics in the heart, Phys. Rep. **543**, 61 (2014).

[12] A. Karma, Physics of cardiac arrhythmogenesis, Annu. Rev. Condens. Matter Phys. **4**, 313 (2013).

[13] G. Bub, A. Shrier, and L. Glass, Spiral wave generation in heterogeneous excitable media, Phys. Rev. Lett. **88**, 058101 (2002).

[14] T. Kiyosue, M. Arita, H. Muramatsu, A. Spindler, and D. Noble, Ionic mechanisms of action potential prolongation at low temperature in guinea-pig ventricular myocytes. J. Physiol. **468**, 85 (1993).

[15] W. J. Crozier, The distribution of temperature characteristics for biological processes; critical increments for heart rates, J. Gen. Physiol. **9**, 531 (1926).

[16] V. V. Fedorov, A. V. Glukhov, S. Sudharshan, Y. Egorov, L. V. Rosenshtraukh, and I. R. Efimov, Electrophysiological mechanisms of antiarrhythmic protection during hypothermia in winter hibernating versus nonhibernating mammals, Heart Rhythm **5**, 1587 (2008).

[17] S. Filippi, A. Gizzi, C. Cherubini, S. Luther, and F. H. Fenton, Mechanistic insights into hypothermic ventricular fibrillation: The role of temperature and tissue size, EP Europace **16**, 424 (2014).

[18] A. Gizzi, A. Loppini, E. Cherry, C. Cherubini, F. Fenton, and S. Filippi, Multi-band decomposition analysis: Application to cardiac alternans as a function of temperature, Physiol. Meas. **38**, 833 (2017).

[19] A. Loppini, A. Barone, A. Gizzi, C. Cherubini, F. H. Fenton, and S. Filippi, Thermal effects on cardiac alternans onset and development: A spatiotemporal correlation analysis, Phys. Rev. E **103**, L040201 (2021).

[20] A. Crispino, A. Loppini, I. Uzelac, S. Iravanian, N. K. Bhatia, M. Burke, S. Filippi, F. H. Fenton, and A. Gizzi, A cross species thermoelectric and spatiotemporal analysis of alternans in live explanted hearts using dual voltage-calcium fluorescence optical mapping, Physiol. Meas. **45**, 065001 (2024).

[21] E. M. Moore, A. D. Nichol, S. A. Bernard, and R. Bellomo, Therapeutic hypothermia: Benefits, mechanisms and potential clinical applications in neurological, cardiac and kidney injury, Injury **42**, 843 (2011).

[22] J. B. Nolasco and R. W. Dahlen, A graphic method for the study of alternation in cardiac action potentials. J. Appl. Physiol. **25**, 191 (1968).

[23] E. M. Cherry and F. H. Fenton, Suppression of alternans and conduction blocks despite steep apd restitution: Electrotonic, memory, and conduction velocity restitution effects, Am. J. Physiol. Heart. Circ. Physiol. **286**, H2332 (2004).

[24] See Supplemental Material at http://link.aps.org/supplemental/10.1103/PhysRevE.111.L012401 for further details on modelling. Specifically SM includes a comprehensive description of the electrophysiological model; the methods used to model the magnetic field; a comparative analysis between magnetic field intensity and action potential time derivative; the numerical methods adopted in simulations. SM also includes Refs. [14,15,20,34,40–42,47].

[25] A. Karma, Spiral breakup in model equations of action potential propagation in cardiac tissue, Phys. Rev. Lett. **71**, 1103 (1993).

[26] A. Garfinkel, Y.-H. Kim, O. Voroshilovsky, Z. Qu, J. R. Kil, M.-H. Lee, H. S. Karagueuzian, J. N. Weiss, and P.-S. Chen, Preventing ventricular fibrillation by flattening cardiac restitution, Proc. Natl. Acad. Sci. USA **97**, 6061 (2000).

[27] J. M. Pastore, S. D. Girouard, K. R. Laurita, F. G. Akar, and D. Rosenbaum, Mechanism linking t-wave alternans to the genesis of cardiac fibrillation, Circulation **99**, 1385 (1999).

[28] B. J. Roth and J. P. Wikswo, Electrically silent magnetic fields, Biophys. J. **50**, 739 (1986).

[29] B. J. Roth, W. Guo, and J. P. Wikswo, The effects of spiral anisotropy on the electric potential and the magnetic field at the apex of the heart, Math. Biosci. **88**, 191 (1988).

[30] R. Plonsey, The nature of sources of bioelectric and biomagnetic fields, Biophys. J. **39**, 309 (1982).

[31] J. R. Holzer, L. E. Fong, V. Y. Sidorov, J. P. Wikswo, and J. F. Baudenbacher, High resolution magnetic images of planar wave fronts reveal bidomain properties of cardiac tissue, Biophys. J. **87**, 4326 (2004).

[32] B. J. Roth, Biomagnetism: The first sixty years, Sensors **23**, 4218 (2023).

[33] B. J. Roth, The magnetocardiogram, Biophys. Rev. **5**, 021305 (2024).

[34] J. F. Barry, M. J. Turner, J. M. Schloss, D. R. Glenn, Y. Song, M. D. Lukin, H. Park, and R. L. Walsworth, Optical magnetic detection of single-neuron action potentials using quantum defects in diamond, Proc. Natl. Acad. Sci. USA **113**, 14133 (2016).

[35] J. L. Webb, L. Troise, N. W. Hansen, C. Olsson, A. M. Wojciechowski, J. Achard, O. Brinza, R. Staacke, M. Kieschnick, J. Meijer *et al.*, Detection of biological signals from a live mammalian muscle using an early stage diamond quantum sensor, Sci. Rep. **11**, 2412 (2021).

[36] F. Baudenbacher, N. Peters, P. Baudenbacher, and J. Wikswo, High resolution imaging of biomagnetic fields generated by action currents in cardiac tissue using a lts-squid microscope, Physica C: Supercond. **368**, 24 (2002).

[37] S. Tanaka, N. Tanaka, M. Natsume, M. Uchida, M. Oshita, Z. Aspanut, T. Eki, and S. Yoshida, Measurement of the signal from a cultured cell using a high-tc squid, Supercond. Sci. Technol. **16**, 1536 (2003).

[38] K. Arai, A. Kuwahata, D. Nishitani, I. Fujisaki, R. Matsuki, Y. Nishio, Z. Xin, X. Cao, Y. Hatano, S. Onoda *et al.*, Millimetre-scale magnetocardiography of living rats with thoracotomy, Commun. Phys. **5**, 200 (2022).

[39] D. Le Sage, K. Arai, D. R. Glenn, S. J. DeVience, L. M. Pham, L. Rahn-Lee, M. D. Lukin, A. Yacoby, A. Komeili, and R. L. Walsworth, Optical magnetic imaging of living cells, Nature (London) **496**, 486 (2013).

[40] F. H. Fenton, A. Gizzi, C. Cherubini, N. Pomella, and S. Filippi, Role of temperature on nonlinear cardiac dynamics, Phys. Rev. E **87**, 042717 (2013).

[41] K. R. Swinney and J. P. Wikswo, A calculation of the magnetic field of a nerve action potential, Biophys. J. **32**, 719 (1980).

[42] F. Fenton and A. Karma, Vortex dynamics in three-dimensional continuous myocardium with fiber rotation: Filament instability and fibrillation, Chaos **8**, 20 (1998).

[43] F. E. Smith, P. Langley, P. Van Leeuwen, B. Hailer, L. Trahms, U. Steinhoff, J. P. Bourke, and A. Murray, Comparison of magnetocardiography and electrocardiography: A study of automatic measurement of dispersion of ventricular repolarization, Europace **8**, 887 (2006).

[44] J. F. Barry, J. M. Schloss, E. Bauch, M. J. Turner, C. A. Hart, L. M. Pham, and R. L. Walsworth, Sensitivity optimization for nv-diamond magnetometry, Rev. Mod. Phys. **92**, 015004 (2020).

[45] E. Moreva, E. Bernardi, P. Traina, A. Sosso, S. D. Tchernij, J. Forneris, F. Picollo, G. Brida, Ž. Pastuović, I. Degiovanni *et al.*, Practical applications of quantum sensing: A simple method to enhance the sensitivity of nitrogen-vacancy-based temperature sensors, Phys. Rev. Appl. **13**, 054057 (2020).

[46] R. Schirhagl, K. Chang, M. Loretz, and C. L. Degen, Nitrogen-vacancy centers in diamond: Nanoscale sensors for physics and biology, Annu. Rev. Phys. Chem. **65**, 83 (2014).

[47] S. A. Teukolsky, B. P. Flannery, W. Press, and W. Vetterling, *Numerical Recipes in C* (Cambridge University Press, 1992).